Injectable body temperature responsive hydrogel for encephalitis treatment via sustained release of nano-anti-inflammatory agents

Yuqi Gai[1,#], Huaijuan Zhou[2,3,#], Yingting Yang[2], Jiatian Chen[1], Bowen Chi[4], Pei Li[5], Yue Yin[1,], Yilong Wang[4,*], Jinhua Li[1,3,*]*

Key Words:
anti-inflammatory nanomedicines; cranial bone defects; encephalitis; injectable hydrogels; sustained release

From the Contents

ABSTRACT

Skull defects are common in the clinical practice of neurosurgery, and they are easily complicated by encephalitis, which seriously threatens the life and health safety of patients. The treatment of encephalitis is not only to save the patient but also to benefit the society. Based on the advantages of injectable hydrogels such as minimally invasive surgery, self-adaptation to irregularly shaped defects, and easy loading and delivery of nanomedicines, an injectable hydrogel that can be crosslinked in situ at the ambient temperature of the brain for the treatment of encephalitis caused by cranial defects is developed. The hydrogel is uniformly loaded with nanodrugs formed by cationic liposomes and small molecule drugs dexmedetomidine hydrochloride (DEX-HCl), which can directly act on the meninges to achieve sustained release delivery of anti-inflammatory nanodrug preparations and achieve the goal of long-term anti-inflammation at cranial defects. This is the first time that DEX-HCl has been applied within this therapeutic system, which is innovative. Furthermore, this study is expected to alleviate the long-term suffering of patients, improve the clinical medication strategies for anti-inflammatory treatment, promote the development of new materials for cranial defect repair, and expedite the translation of research outcomes into clinical practice.

***Corresponding authors:**
Jinhua Li,
lijinhua@bit.edu.cn;
Yilong Wang,
yilongwang528@163.com;
Yue Yin,
yinyue@bit.edu.cn.

#Authors equally.

http://doi.org/10.12336/biomatertransl.2024.03.006

How to cite this article:
Gai, Y.; Zhou, H.; Yang, Y.; Chen, J.; Chi, B.; Li, P.; Yin, Y.; Wang, Y.; Li, J. Injectable body temperature responsive hydrogel for encephalitis treatment via sustained release of nano-anti-inflammatory agents. *Biomater Transl.* **2024**, *5*(3), 300-313.

Introduction

The brain is the most important organ in the human body, managing both the outside and the inside.[1, 2] In neurosurgical practice, open-head trauma is very common, and it mainly stems from some risk factors in life. In addition, patients have various reasons why craniotomy is necessary, which is also an important cause of skull defects. All of these can lead to encephalitis infection.[3] Encephalitis is a global disease with a high mortality rate.[4, 5] According to the Encephalitis International, one person gets encephalitis every minute on average, yet 80% of people do not know what encephalitis is.[6]

Encephalitis is an inflammatory response to the brain parenchyma, and this inflammatory lesion is clinically characterised by typical encephalopathy symptoms.[3, 7] Encephalitis can also cause severe neurological sequelae as shown in **Figure 1A**.[8, 9] This has a great impact on the safety of human life and quality of life, and may even affect the stability of society.[10, 11] Hence, the treatment of encephalitis is crucial. For encephalitis caused by cranial defects, the traditional treatment methods are mainly symptomatic treatment, but the treatment direction is not targeted.[12-14] Therefore, there is an urgent need for novel therapeutic approaches to target the cranial defect for protection and long-term anti-inflammatory therapy.

At present, many targeted drug delivery systems can break through the blood-brain barrier in the field of central nervous system (CNS) drug

delivery,[15-20] such as exosomes,[21] membrane-coated drugs,[22, 23] and bioactive lipophilic small molecule drugs.[24] However, poor stability, short half-life and complex production process still need to be improved. Although drugs acting directly on the CNS can overcome the above shortcomings, they are again highly likely to have serious adverse drug reactions and drug toxicity. Therefore, it is necessary to explore an ideal drug delivery technology that is not only capable of treating diseased sites within the CNS, but also sufficiently rapid, safe and effective. With the development of nanotechnology in the biomedical field, there have been some studies on nanodrug delivery technology, which have shown unique advantages such as optimising pharmacokinetics,[25] improving the duration of drug action,[26] and reducing the total amount of drug use.[27] There are many types of nanoparticles, and the selection of carrier type and delivery method according to the type of drug is expected to achieve safe and accurate delivery of drugs.[28-30]

For a brief overview of the damage to the brain caused by encephalitis, as illustrated in **Figure 1B**, using the CNS inflammatory factor storm as an example, neuroglial cells are actively involved in this process.[31] Cells in the CNS secrete inflammatory factors when they are damaged, which not only activate inflammatory microglia[32-34] and astrocytes[35, 36] but also attract and activate leukocytes in the peripheral circulation. More inflammatory factors continue to accumulate in the CNS,[37-39] further exacerbating the severity of encephalitis.[40] Therefore, there is demend to intervene in the abnormal inflammatory response within the CNS. The anti-inflammatory agents commonly used for the treatment of encephalitis are glucocorticoids,[41] but due to their wide range of actions, high doses or prolonged application can cause a variety of adverse effects, hence there is a need to find alternatives.

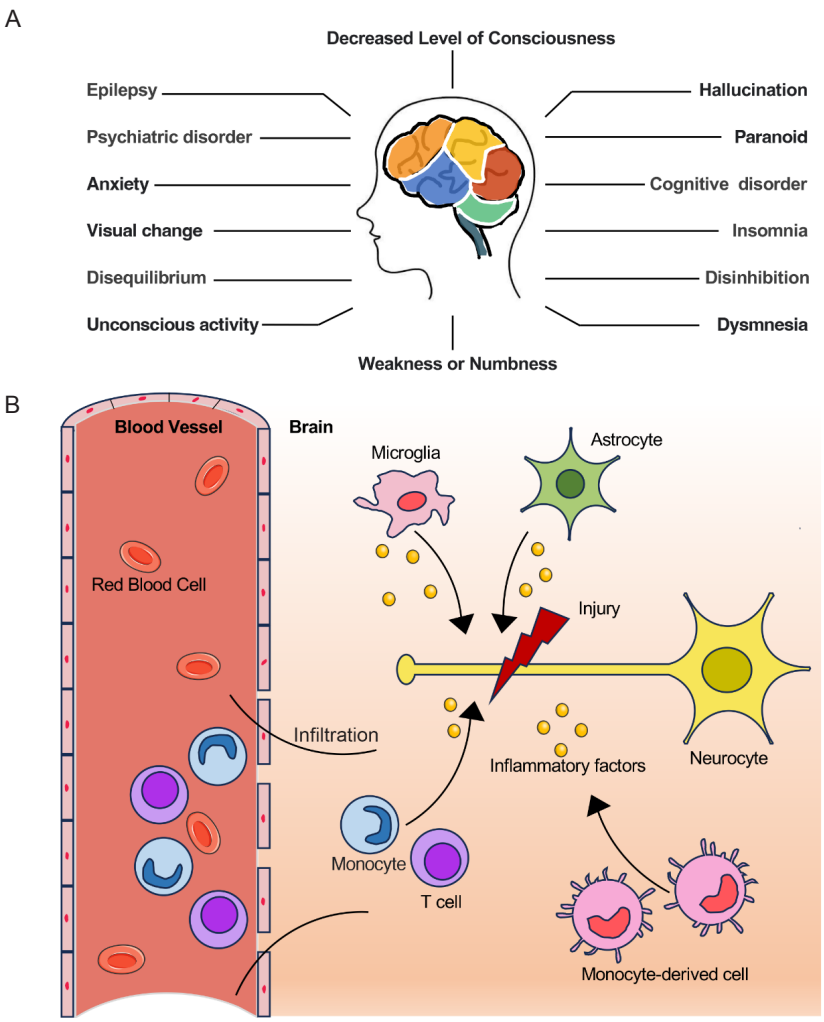

Figure 1. Schematic diagram of encephalitis symptoms. (A) Encephalitis can cause varying degrees of neurological deficit in patients. (B) The accumulation of inflammatory factors in the brain of patients with encephalitis. Created with Microsoft PowerPoint 2021.

1 School of Medical Technology, Beijing Institute of Technology, Beijing, China; 2 Advanced Research Institute of Multidisciplinary Sciences, Beijing Institute of Technology, Beijing, China; 3 Beijing Institute of Technology, Zhuhai, Beijing Institute of Technology (BIT), Zhuhai, Guangdong Province, China; 4 Department of Neurology, Beijing Tiantan Hospital, Capital Medical University, Beijing, China; 5 Center for Advanced Biotechnology & Medicine, Rutgers University, Piscataway, NJ, USA

Studies have shown that, A1-reactive astrocytes induced under inflammatory conditions sustainably release inflammatory cytokines that destroy nerve cells.[42, 43] A2-reactive astrocytes induced under ischaemic conditions can nourish nerve cells and promote repair. Dexmedetomidine hydrochloride, an α2-adrenergic receptor agonist, has been found to inhibit neuroinflammation and promote the change of astrocyte subtype from A1 to A2.[37, 44]

Based on the above ideas, as shown in **Figure 2**, we designed an injectable hydrogel precursor loaded with liposomal nano-anti-inflammatory drugs, which can be used to treat encephalitis in the state of cranial defects. The precursor is a chitosan (CS)-based thermosensitive hydrogel that enables *in situ* cross-linking at the physiological temperature in the brain. By bypassing the blood-brain barrier and directly contacting brain tissue,[45, 46] anti-inflammatory drugs are continuously released in the brain, promoting the transformation of astrocytes from type A1 to type A2, which is expected to inhibit CNS inflammation and reduce patient suffering. The aim of this experiment was to successfully prepare brain nano-anti-inflammatory drug sustained-release injectable hydrogels with biocompatibility, biosafety, delivery efficiency and therapeutic feasibility. It provides solid technical support and theoretical direction to promote subsequent research and development.

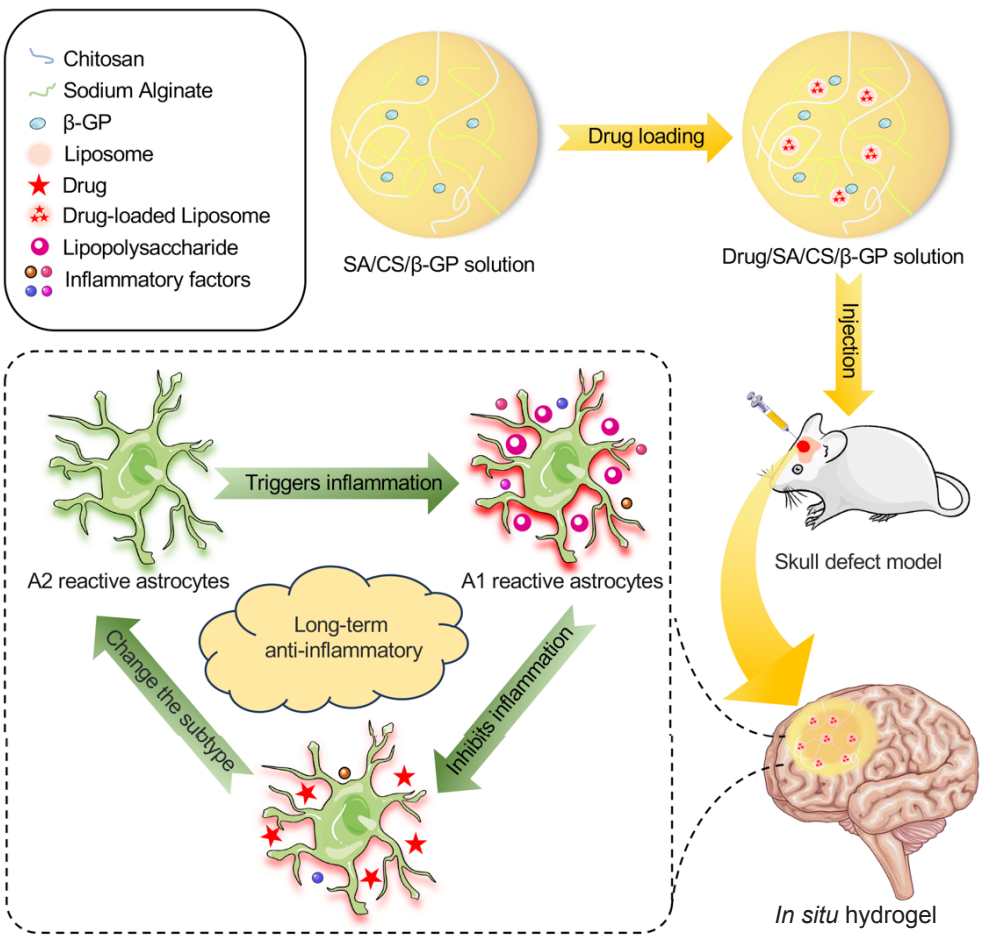

Figure 2. Schematic diagram of drug action. Preparation of an injectable chitosan-based thermosensitive hydrogel for long-term sustained drug release for the treatment of cerebral inflammation. Created with Microsoft PowerPoint 2021. CS: chitosan; SA: sodium alginate; β-GP: β-glycerophosphate.

Methods

Synthesis of drug-loaded liposomes

The classical thin-film dispersion method was used to prepare drug-loaded liposomes (referred to as +lipo).[47, 48] Initially, 10 phosphate buffer saline (PBS; Solarbio, Shanghai, China) was diluted with water to 1× PBS, and PBS was used to configure separate doxorubicin hydrochloride (DOX-HCl; MREDA, Beijing, China) and dexmedetomidine hydrochloride (DEX-HCl; Aladdin, Shanghai, China) solutions at a concentration of 1 mg/mL (referred to as +free).

Subsequently, lipid solutions were prepared by dissolving D-Lin-MC3-DMA (Aladdin) and cholesterol (Solarbio) in anhydrous ethanol (Aladdin) at a ratio of 6:1. Following rotary evaporation (R-1001VN, Greatwall, Zhengzhou, Henan, China) of the organic phase, an appropriate amount of previously prepared +free was added, and sonicated for about 10 minutes. The sonicated solution was transferred to an ultrafiltration centrifuge tube (Amicon Ultra-4, Millipore, Billerica, MA, USA) and centrifuged at 2500 × *g* for 20 minutes to collect +lipo.

Synthesis of drug loaded hydrogel precursors

We used CS-based temperature-sensitive hydrogels, which are often employed in investigating drug release mechanisms.[49, 50] The hydrogels were prepared by initially weighing and dissolving an appropriate amount of CS (Adamas Life, Shanghai, China) and sodium alginate (SA; Adamas Life) in 1% (v/v) acetic acid aqueous solution and distilled water, respectively. Magnetic stirring was then used to obtain 2% (w/v) solutions of both CS and SA. Subsequently, β-glycerophosphate (β-GP, Sigma-Aldrich Corp., St. Louis, MO, USA) was weighed and dissolved in distilled water to produce a 56% (w/v) solution. The β-GP solution was slowly added dropwise to the CS solution under a 4°C ice bath, following a ratio of $V_{β\text{-}GP}$:V_{CS} = 0.3:1, resulting in the CS/β-GP mixed solution after 30 minutes of magnetic stirring. Likewise, equal amounts of CS/β-GP mixed solution and SA solution were combined and stirred for another 30 minutes to form a mixed SA/CS/β-GP solution, denoted as the blank hydrogel precursor (referred to as blank gel). To introduce drugs, the blank gel was supplemented with +free and +lipo, yielding the free gel and lipo gel, respectively. The methyl orange staining step was used in the preparation of the hydrogel precursor solution, which was added to the precursor solution in advance at 4°C to allow it to be homogeneously mixed and facilitated by the visualization of the hydrogel.

Characterisation of materials

Structural characteristics of liposome and hydrogel materials were investigated through a series of experiments.[26, 51, 52] Liposome morphology and size were analysed using the transmission electron microscope (JEM-1400 Plus, JEOL LTD., Tokyo, Japan), while the zeta potential analyzer Zetasizer Nano (Malvern Panalytical Ltd., Malvern, UK) provided information on particle size and distribution. Additionally, fluorescence intensities of +free and +lipo were measured with the microplate reader (Cytation 3, BioTek, Vermont, VT, USA). The encapsulation efficiency (DLE) and drug-loading rate (DLC) for +lipo were calculated according to equations 1 and 2:

$$DLE\ (\%) = \left(\frac{C_1}{C_2}\right) \times 100 \quad (1)$$

$$DLC\ (\%) = \left(\frac{C_1}{C_1+C_0}\right) \times 100 \quad (2)$$

In the formulae: C_1 represents the amount of loaded drug, C_2 represents the amount of input drug, and C_0 represents the amount of carrier.

The cross-linking state and timing of the hydrogel were then observed according to a standardised protocol. The hydrogel precursor was placed upright in tube in a 37°C water bath to monitor the cross-linking process. Successful cross-linking was indicated when the gel was stable and did not slide off when the tube was inverted. The gelation time at this temperature was recorded, and the procedure was repeated thrice, with an average value calculated. Subsequently, the hydrogel was pre-frozen in liquid nitrogen for 12 hours and then subjected to a 24-hour freeze-drying process. The scanning electron microscope (Apreo C, Thermo Fisher Scientific, Waltham, MA, USA) was used to observe the pore size and morphology of both blank and drug-loaded hydrogels, while the Young's modulus were determined using rheometer (HAAKE MARS 40, Thermo Fisher Scientific).

Drug release study

In this *in vitro* simulated physiological environment, DOX-HCl, a widely used anti-cancer drug, functioned as the model drug to replace DEX-HCl, primarily due to the absence of characteristic groups and fluorescence in DEX-HCl, rendering the application of an appropriate detection method implausible.[53, 54] DOX-HCl and DEX-HCl are two completely different drugs, and in order to assess whether DOX-HCl could be used as a model drug in the preliminary phase of this study, the two were compared for certain similarities in their physicochemical properties and release mechanisms. In terms of physicochemical properties, DOX-HCl has a molecular weight of about 579.98 g/mol and DEX-HCl has a molecular weight of about 236.72 g/mol, which are both considered small molecules despite the difference in molecular weights, and both DOX-HCl and DEX-HCl are hydrophilic and have high solubility in water. For the release mechanism, this experiment envisages the use of the drug encapsulated in a liposomal system. Since both are water soluble drugs, they are usually released from the carrier by diffusive release. This means that the rate of movement of drug molecules in the carrier is limited by the rate of diffusion. The mechanism of release may then be similar for both of them.

The drug release ability of drug-loaded hydrogels was assessed by the observation of the gradual release of the model drug from both the free gel and lipo gel under an inverted microscope (ECLIPSE Ti2-E, Nikon Corporation, Tokyo, Japan). Subsequently, the fluorescence intensity of DOX-HCl released from the free gel and lipo gel was quantified using the microplate reader and the ensuing data was subjected to processing and analysis. It is noteworthy that the excitation wavelength of DOX-HCl was determined to be 495 nm, while its emission wavelength was measured at 595 nm.

In vitro cytotoxicity

Mouse astrocytes-cerebellar (MA-c, BeNa Culture Collection Co. Ltd, Beijing, China) were first seeded at a density of 1 × 10^4/mL in 96-well plates. Cells were cultured in DMEM medium(Gibco, Carlsbad, CA, USA) containing 10% FBS (Gibco, Carlsbad, CA, USA) for 24 hours at an ambient temperature of 37°C and a CO_2 concentration of 5%. Following this incubation period, the biosafety evaluation was assessed

for the blank hydrogel group, +free group, and +lipo group, in which the drug loaded in the +free and +lipo groups was DEX-HCl. Hydrogels at concentrations of 0, 1, 10, 50, and 100 g/mL, +free at 0, 1, 5, 10, and 20 μg/mL, and +lipo at 0, 1, 5, 10, and 20 μg/mL were added to the corresponding experimental wells and co-cultivated with the cells for 24 hours. The +free and +lipo groups were loaded with DEX-HCl. Subsequently, 10 μL of cell counting kit-8 (Analysis Quiz, Beijing, China) solution was added to each well. After 2 hours of incubation, the absorbance at 450 nm was measured using the microplate reader, and the results were processed and analysed for further evaluation of biosafety.

Cellular uptake of drugs

The uptake of liposome-encapsulated DOX-HCl by MA-c cells was evaluated using both qualitative and quantitative methods. For qualitative analysis, cells were cultured in the presence of +free and +lipo, treated with 4',6-diamidino-2-phenylindole (Beyotime, Shanghai, China) staining and Lyso-Tracker Red (Beyotime) staining, and examined under a confocal laser microscope (N-SIM E, Nikon Corporation) to visualize the distribution of fluorescently labelled areas. Concurrently, the quantitative analysis involved co-culturing cells with blank control, +free, and +lipo, followed by flow cytometry using a FACSAria II (BD Biosciences, Franklin Lakes, NJ, USA) to quantify the amount of DOX-HCl uptake by the respective groups of cells.

Cell subtype transition

Experiments were conducted to establish the modelling concentration of lipopolysaccharide (LPS, Beyotime), a distinctive component of the cell wall of Gram-negative bacteria often utilised in inflammation stimulation in mouse models.[55, 56] In order to determine the appropriate concentration, LPS was co-cultured with MA-c in a gradient spanning from low to high concentrations for 24 hours (1, 5, and 10 μg/mL), followed by the assessment of the expression levels of inflammation-related genes within the cells. Subsequently, various techniques were employed to evaluate the capacity of inflammatory cell subtypes to be successfully and efficiently altered in response to the drug.

Quantitative polymerase chain reaction

MA-c cells were seeded at a density of 2×10^6/mL in a 6-well plate, followed by a 24-hour culture under normal cell culture conditions. The cells were then divided into two groups: one served as a blank control group while the other was exposed to a culture environment containing 10 μg/mL LPS. Subsequently, after 24 hours, the LPS-treated cells were further subdivided into three groups: the first group remained unchanged, the second group was transferred to a new culture environment with 2.0 μg/mL + free, and the third group was exposed to a new culture environment with 2.217 μg/mL + lipo. Notably, each cell group had three replicates, ensuring the reliability of the results obtained. Following the cell culture, cells and cell culture supernatants from each group were collected, and all subsequent experimental procedures were carried out on ice to maintain sample integrity.

The experimental operations were conducted meticulously in accordance with the RNA extraction kit instructions (BioSharp, Hefei, Anhui, China). This involved lysing the cells thoroughly, removing impurities such as mixed genomic DNA and proteins through centrifugation, washing, and filtration processes, ultimately resulting in the extraction of total RNA solutions. Subsequently, the RNA concentration in each group was determined using a microvolume ultraviolet spectrophotometer (NanoDrop Lite Plus, Thermo Fisher Scientific), and adjustments were made to ensure uniform RNA concentrations across all groups. Furthermore, the synthesis of cDNA was performed following the guidelines of the reverse transcription kit (BioSharp). A precise mixture of the RNA template, SuperRT III All-in-one RT Mix, SuperRT III All-in-one RT Buffer, and Nuclease-free Water was prepared and utilised to synthesize cDNA in a gene amplification instrument (Gene Explorer, Bioer Technology, Hangzhou, Zhejiang, China).

Subsequently, following the protocol of the universal quantitative polymerase chain reaction (qPCR) kit (BioSharp), a proportional mix of the cDNA template, 2× Universal SYBR qPCR Mix, primers (Sangon Biotech Co., Ltd., Shanghai, China), ROX Reference Dye, and RNase-Free ddH_2O was prepared and subjected to real-time PCR analysis using a Real-time PCR amplification (Applied Biosystems QuantStudio 5 instrument, Thermo Fisher Scientific). The relative expression of the genes of interest was normalised against the housekeeping gene *Gapdh*. Primer sequences were as follows: *H2-T23*: forward, 5'-TGA TCA TCC TTG GAG CTG TG-3', reverse, 5'-TTC TGA GGC CAG TCA GAG GT-3'; *H2-D1*: forward, 5'-GTT GCT GTT CTG GGT GTC CT-3', reverse, 5'-CCT GGA GCC AGA GCA TAG TC-3'; *Tgm1*: forward, 5'-CCC TGG ATG ACA ATG GAG TT-3', reverse, 5'-GAA TAG CCG GTG CGT AGG TA-3'; *S100a10*: forward, 5'-GTG CTC ATG GAA CGG GAG T-3', reverse, 5'-AAA GCT CTG GAA GCC CAC TT-3'; and *Gapdh*: forward, 5'-TCA CCA TCT TCC AGG AGC GAG AC-3', reverse, 5'-AGA CAC CAG TAG ACT CCA CGA CAT AC-3'.

Enzyme-linked immunosorbent assay

In this trial, the double-antibody sandwich method was used as the core technology of enzyme-linked immunosorbent assay (ELISA) kit (Lianke, Hangzhou, Zhejiang, China), and the test was carried out strictly according to the protocol. To begin, the cell culture supernatant stored at –20°C was removed and allowed to return to room temperature. Steps included rinsing the plate pre-coated with capture antibody, adding samples to the plate wells, and incubating with biotinylated detection antibody at room temperature for approximately 2 hours. The next steps included discarding the solution, washing the plate, adding horseradish peroxidase-labelled streptavidin, and incubating at room temperature for 45 minutes, then discarding the solution again and washing the plate. Subsequently, the chromogenic substrate was added, with precautions taken to protect it from light. After half an hour, the stop solution was introduced to halt the reaction. Finally, the absorbance values were measured by measuring at 450 and 630 nm using the microplate reader for analysis.

Western blot analysis

Western blotting combines the high resolution of protein electrophoresis with the high specificity of immunoassays.[57] In the early stage of the experiment, the cell group culture and dosing were consistent with the qPCR experiment. Subsequent experimental procedures were conducted at 4°C on ice. Cells were collected and lysed using RIPA lysate (Analysis Quiz) containing protease inhibitors (Analysis Quiz) to extract proteins. The original protein concentrations in each group were determined using NanoDrop, and then adjusted to ensure uniformity across groups. Afterward, the proteins were combined with 5× sample loading buffer (Applygen Technologies Inc., Beijing, China) and heated in a metal dry bath heater (HB120-S, DLAB, Beijing, China) at 95°C for 5 minutes. Following, an aliquot of the sample was prepared and subjected to electrophoresis (Mini-PROTEAN Tetra, Bio-Rad Laboratories Inc., Hercules, CA, USA) using 10% sodium dodecyl sulfate-polyacrylamide gel electrophoresis gel kit (Analysis Quiz). The gel, filter paper, sponge, and polyvinylidene fluoride membrane (Solarbio) were assembled and clamped for transfer (Mini Trans-Blot, Bio-Rad Laboratories Inc.).

Subsequently, the polyvinylidene fluoride membrane was blocked with skim milk (Analysis Quiz) at room temperature for 1 hour, followed by overnight incubation at 4°C with rabbit monoclonal anti-high mobility group box 1 (HMGB1) antibody (1:2000, Cat# ab92310, RRID:AB_2049739 Abcam, Cambridge, UK) and rabbit monoclonal anti-α-tubulin antibody (1:10,000, Abcam, Cat# ab52866, RRID:AB_869989). After incubation with the primary antibodies, the membrane was treated with goat anti-rabbit IgG H&L (HRP) (1:5000, Huaxingbio, Beijing, China, Cat# HX2031, RRID:AB_3572247) for 1 hour at room temperature. The chemiluminescence signal was developed using an ECL mixture kit (Analysis Quiz), and the blots were visualised and imaged using a fully automatic gel imager (iBright CL1500, Thermo Fisher Scientific). Finally, protein bands were analysed semiquantitatively. The protein expression of HMGB1 was calculated by normalising to α-tubulin.

Statistical analysis

All experimental data were presented as mean ± standard deviations (SDs). Data analysis were performed using GraphPad Prism 6 (GraphPad Software, Boston, MA, USA, www.graphpad.com) and ImageJ software (National Institutes of Health, Bethesda, MD, USA). Statistical significance was assessed using Student's *t*-test for comparisons between two groups and one-way analysis of variance with Newman-Keuls *post hoc* test for multiple group comparisons. Statistical significance levels were defined as $P < 0.05$.

Results

Characterisation of +lipo and hydrogel

The characterisation results of liposome nanoparticles and CS hydrogels were shown in **Figure 3**. Under the transmission electron microscope, +lipo nanoparticles were homogeneous in structure and spherical vesicles with an average particle size of about 200 nm (**Figure 3A**). The average particle size of the nanoparticles was about 183.7 ± 54.1 nm, which was narrowly distributed (**Figure 3B**). The zeta potential of the nanoparticles was +11.4 ± 0.8 mV by electrophoretic light scattering. According to the analysis of the microplate reader data, the DLE of +lipo was measured to be about 90.2 ± 6.2% and the DLC was about 47.4 ± 1.7%.

Hydrogel characterisation results were shown in **Figure 3C–E**. As shown in **Figure 3C**, a comparison of macroscopic images of the hydrogel before and after gelation, the hydrogel precursor gel gelled in about half an hour at 37°C, and the gel was stained with methyl orange for the purpose of making it easier to observe with the naked eye. **Figure 3D** showed the scanning electron microscope images of hydrogel. The lyophilised hydrogels had three-dimensional porous surface structure with pore sizes ranging from about 30 to 100 μm. The lipo gel group had a more pronounced pore structure than the free gel group, which may be caused by the loading of +lipo. **Figure 3E** showed the Young's modulus with time. Both blank gel and lipo gel groups had a larger G' than G", proving the formation of a stable hydrogel. The Young's modulus gradually decreased over time, indicating that the strength of the material gradually increased with gelatinisation.

Evaluation of *in vitro* release of the drug-loaded hydrogel

Figure 4A showed the gradual release of DOX-HCl from free gel and lipo gel in PBS, with the center group being the gel region and the boundary group being the junction region of the gel and solution. It could be seen that at the very beginning, the inside of the gel was uniformly red, filled with DOX-HCl, and the surrounding PBS was black, without DOX-HCl, and the red and black boundaries were clear. After 24 hours, the red colour inside the gel gradually became lighter, many obvious red spots appeared in the lipo gel group, the surrounding black area began to appear reddish, and the boundary between red and black began to blur. After 48 hours, the red colour inside the gel became lighter, and the lipo gel group still had obvious red spots, the surrounding black area was pale red, and the boundary between red and black was more blurred. This indicates that the gel continuously releases DOX-HCl into PBS, and the red dot should be +lipo, because the liposome encapsulates the drug, so the lipo gel group has more aggregated DOX-HCl and more red dots.

Figure 4B showed the drug release profiles of DOX-HCl from the free gel and the lipogel over time. The release experiments were performed at 37°C and the obtained release data were analysed by curve fitting. The results showed that the cumulative release rate of the free gel group reached 2.4% over a total of 4 days, which was about four times that of the lipo gel group. The drug in the free gel group showed a rapid initial release phase followed by a smooth phase of slower release. This suggests that the carrier is controllable for drug release and is consistent with the characteristics of a one-level release kinetic model. The drug in the lipo gel group remained in a smooth phase of slow release, which is consistent with the characteristics of the zero-level release kinetic model, which reflects that the lipo gel group has the advantages of sustained and controlled release that the free gel group does not have.

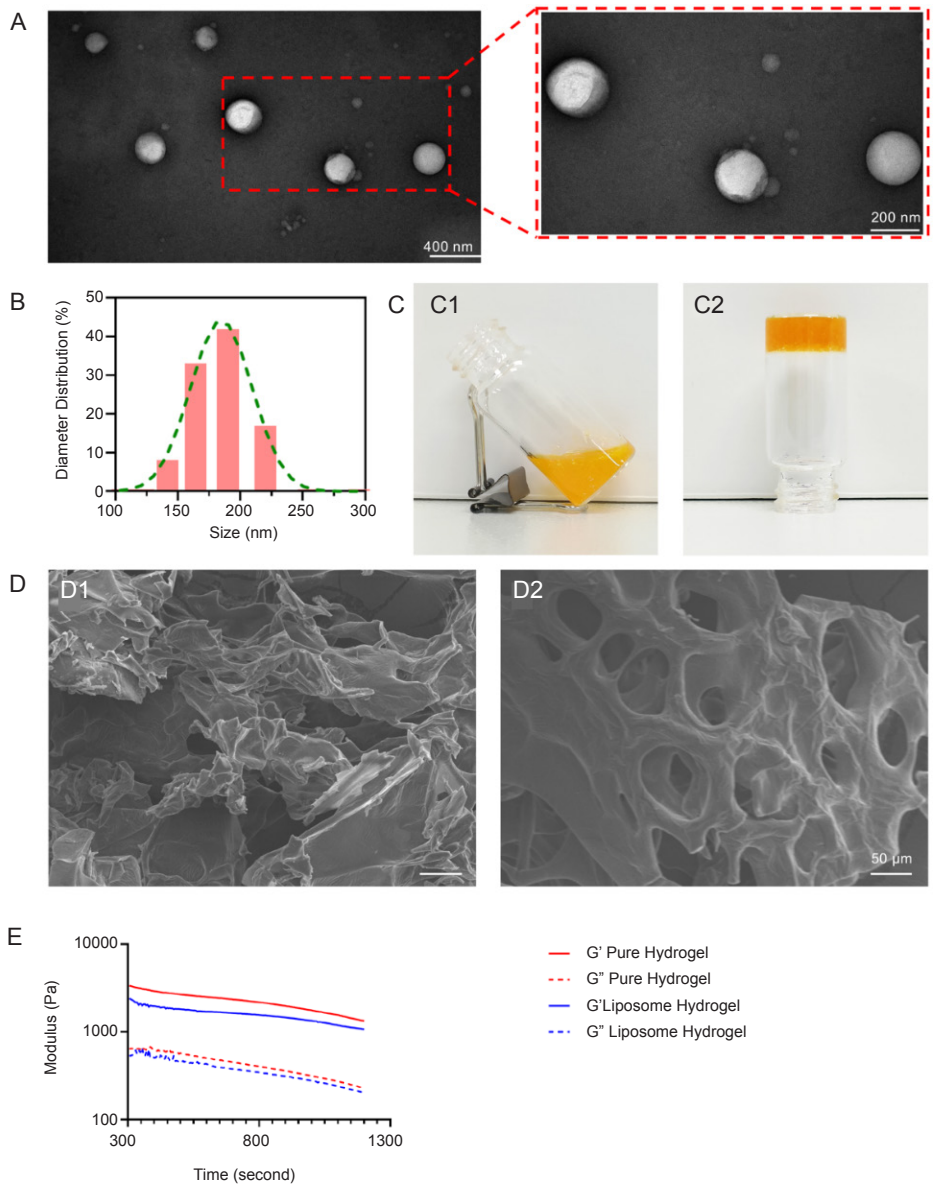

Figure 3. Basic characterisation of materials. (A) Morphology of drug-loaded liposomes, which were uniformly spherical in shape. (B) Particle size distribution of drug-loaded liposomes. (C) Photos of hydrogel formation. (C1) Before gel formation; (C2) after gel formation. (D) Internal 3D structure of hydrogel. (D1) pure hydrogel; (D2) liposome-loaded hydrogel. The liposome-loaded hydrogel had finer and more regular cavities than pure hydrogel. (E) The mechanical properties of hydrogels. 3D: three-dimensional; *G'*: solid line representing the storage modulus; *G"*: viscous modulus.

Evaluation of *in vitro* cell uptake biological testing

Evaluation of drug-loaded hydrogels for in vitro safety

The cell counting kit-8 method was used to study the *in vitro* cytotoxicity of materials using MA-c cells. As shown in **Figure 5A1–3**, cell viability fluctuated around 100% in each group, The +lipo group even exceeding 100%. The above results showed that blank gel, +free, and +lipo had no adverse effect on the cell viability of cells, and the safety of the materials was verified.

Evaluation of the uptake of model drugs by MA-c cells

Figure 5B showed the confocal image analysis of MA-c cells, which showed that the DOX-HCl of the liposomal drug group was more concentrated in the lysosomal location, while the distribution in the cells of the free drug group was relatively loose.

As shown in **Figure 5C1 and C2**, the relative cell numbers of the control group, the +free group, and the +lipo group at different fluorescence signal relative intensities were shown. Because no DOX-HCl was added to the control group, there was a clear difference in fluorescence intensity from the other two groups. The liposomal drug group had a slightly stronger fluorescence intensity than the free drug group, probably because the cells took up the liposomal drug slightly stronger.

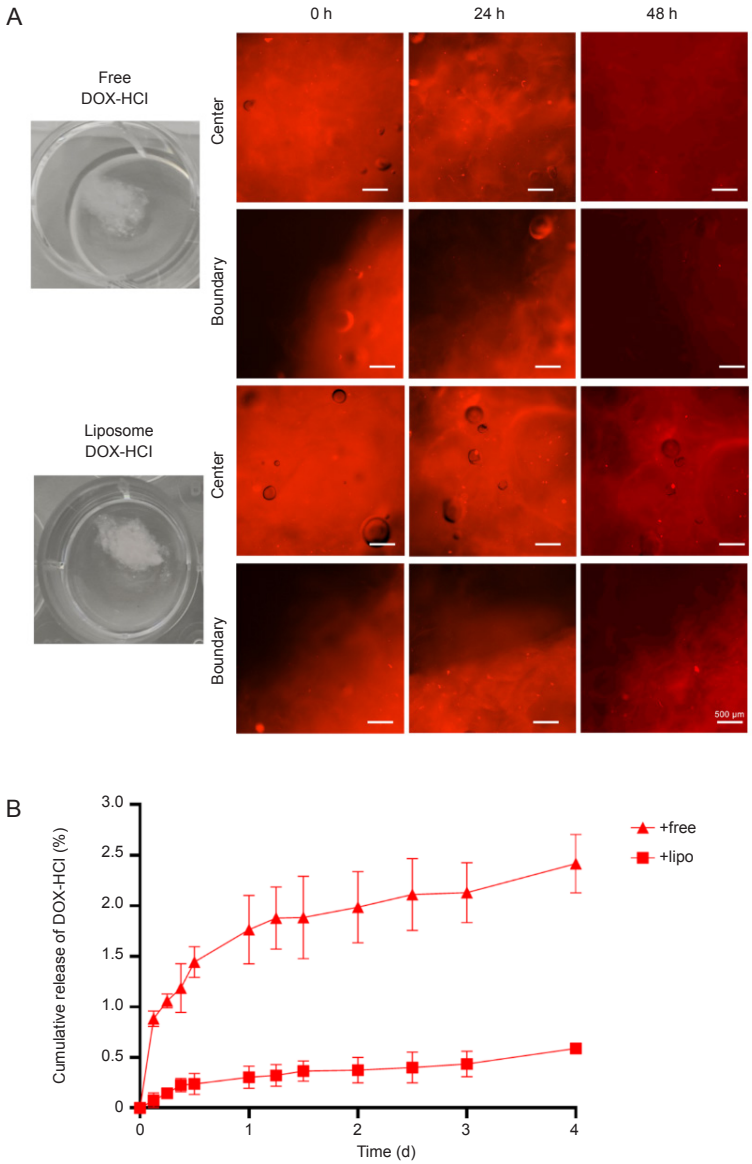

Figure 4. Drug release from hydrogel. (A) Photograph of the gradual release of the model drug from the hydrogel. The liposomal drug group released the drug more slowly than the free drug group, and more of the drug remained stored in the liposomes. Scale bars: 500 μm. (B) Drug release curve of in the hydrogel. Data are expressed as mean ± SD. Experiments were conducted in quadruplicate. +free: free DOX-HCl in the hydrogel; +lipo: liposome DOX-HCl in the hydrogel; DOX-HCl: doxorubicin hydrochloride.

Figure 5C3 showed that the experimental group had a high degree of uptake of DOX-HCl compared with the control group, and there was no significant difference between the free DOX-HCl and liposome DOX-HCl groups. In summary, MA-c cells had a higher uptake intensity of both free drugs and liposomal drugs, but the distribution of liposomal drugs in cells was more concentrated.

Evaluation of *in vitro* cell subtype conversion

Evaluation of MA-c inflammatory subtype modelling

At first, MA-c cells were induced by low concentration (1 μg/mL) of LPS. qPCR results that the expression levels of pro-inflammatory genes *H2-T23* and *H2-D1* were different from the expected results, and there was almost no expression. Therefore, after increasing the concentration of LPS, the expression of inflammatory genes was observed again, and it was found that compared with the low concentration of LPS group, the expression level of pro-inflammatory genes also increased with the increase of LPS concentration, and the expression of anti-inflammatory genes *Tgm1* and *S100a10* almost did not change, which was in line with experimental expectations. Ultimately, it became clear that a higher LPS (10 μg/mL) concentration was required to induce MA-c inflammation (**Additional Figure 1**).

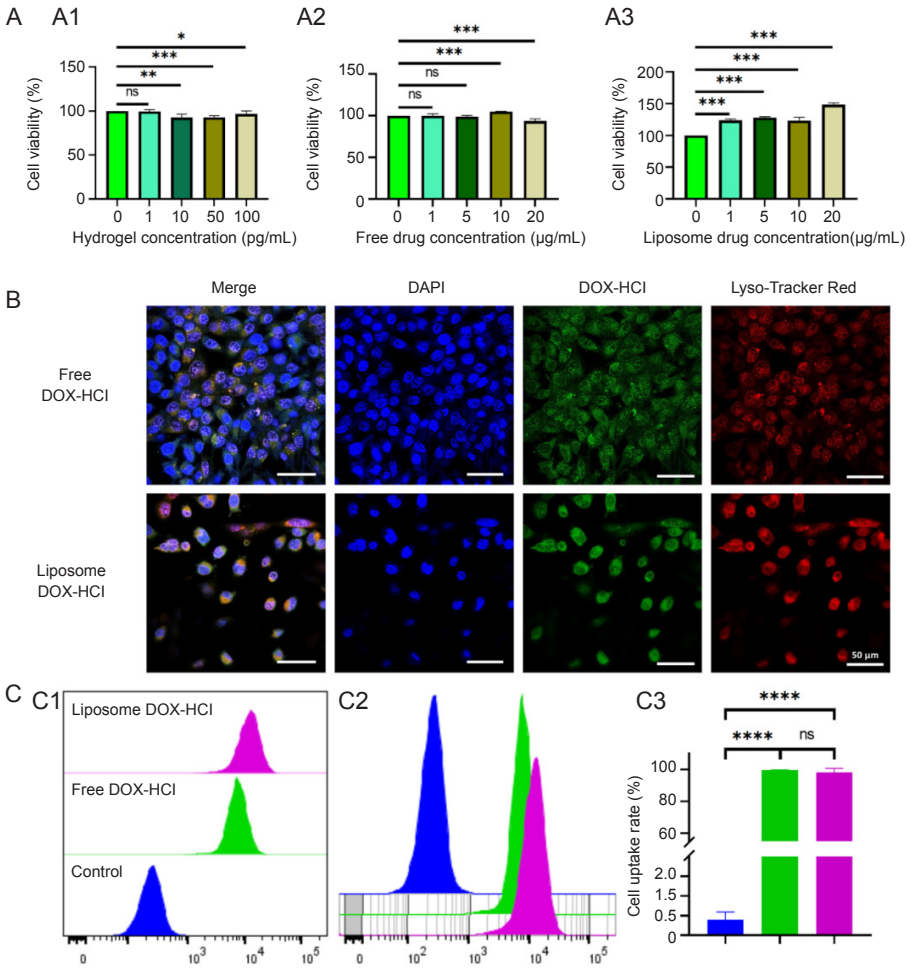

Figure 5. *In vitro* cell uptake biological testing. (A) Cytotoxicity tests of different experimental materials, blank gel (A1), +free (A2), and +lipo (A3). (B) Confocal image of a model drug for cell uptake, with blue for nucleus localization, red for lysosomes, and green for DOX-HCl. It can be seen that drug-loaded liposomes were more likely to be enriched in the cells. Scale bars: 50 μm. (C) Flow cytometry was used to determine the amount of model drug uptaken by cells. (C1, 2) represent the relative cell amounts of the model drug uptake by different cell groups. (C3) Cell uptake rate. Data are expressed as mean ± SD. Experiments were conducted in quadruplicate. *$P < 0.05$, **$P < 0.01$, ***$P < 0.001$, ****$P < 0.0001$ (Student's *t*-test). DAPI: 4',6-diamidino-2-phenylindole; DOX-HCl: doxorubicin hydrochloride; ns: not significant.

Evaluation of treating astrocytic inflammatory subtypes

As shown in **Figure 6A**, it can be seen that the number of cells gradually increases with the number of culture days. The initial MA-c cells were spindle-shaped and polygonal in shape, with long protrusions extending all around. After adding LPS, the cell processes became thicker and shorter, the cell body became round, and the cytoplasm became somewhat turbid, and the rate of cell growth slowed down. Finally adding the therapeutic drugs, +free and +lipo, the cells re-extended their protrusions and their cytoplasm became clear, and the rate of cell growth resumed.

The gene expression levels of the MA-c cell groups at the above different stages were then evaluated by qPCR. First, **Figure 6B1–4** showed the expression levels of A1-reactive astrocyte-specific genes *H2-T23* and *H2-D1* were significantly increased compared with the control group after high-concentration LPS induction, while the expression levels of A2-reactive astrocyte-specific genes *Tgm1* and *S100a10* were significantly reduced, indicating the success of inflammatory modelling. After the administration of the treatment, the expression levels of *H2-T23* and *H2-D1* were significantly reduced compared with the LPS group, while the expression levels of *Tgm1* and *S100a10* were significantly increased, indicating the successful transition of cells from A1 to A2 subtype. The expression levels of *H2-T23* and *H2-D1* were significantly reduced in the cell group supplemented with +lipo compared to the cell group supplemented with +free, while there was no difference in the expression levels of *Tgm1* and *S100a10*, indicating that both treatments reduced the inflammatory expression of cells, but +lipo was more effective than +free.

Second, ELISA also showed similar expression levels to inflammatory genes (**Figure 6B5–8**). Compared with the control group, the expression of interleukin (IL)-1β, IL-6 and tumour necrosis factor (TNF)-α was significantly enhanced

in the LPS group, which once again proved the success of inflammatory modelling. After the administration of the therapeutic drug, the expression levels of inflammatory cytokines were significantly lower compared with the LPS group, which indirectly indicated the successful transition of cells from the A1 subtype to the A2 subtype. The expression levels of IL-1β, IL-6 and TNF-α were significantly lower in the cell group supplemented with +lipo compared to the cell group supplemented with +free, indicating that both treatments reduced the inflammatory expression of the cells, but +lipo was more effective than +free.

Finally, this conclusion was proved by Western blot (**Figure 6B9, 10**) The protein expression of HMGB1 in the LPS group was higher than control group, indicating the success of inflammatory modelling. After the administration of the therapeutic drug, the protein expression of HMGB1 decreased in the free drug and liposome drug groups compared with LPS group, indicating that the expression of inflammatory protein was inhibited. The protein expression of HMGB1 was lower in the liposome drug group compared to the free drug group, indicating that both treatments reduced the inflammatory expression of the cells, but the effect of +lipo was better than that of +free, which was in line with the expected conclusions. In conclusion, it can be inferred that +lipo is more effective in modulating the subtype of MA-c cells and suppressing cellular inflammatory responses when compared to +free.

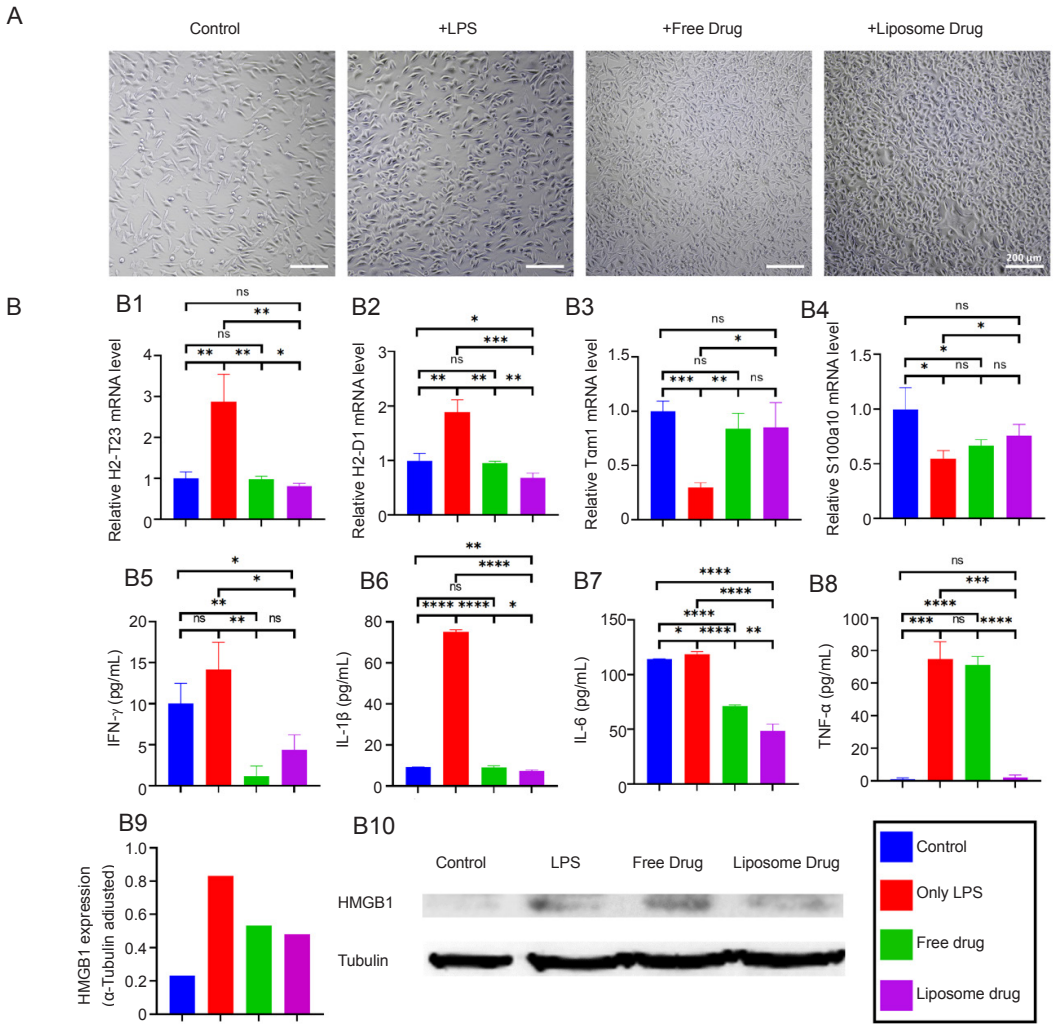

Figure 6. *In vitro* phenotypic conversion of MA-c cells from the A1 subtype to the A2 subtype. (A) Cell morphology at different stages. After the effect of LPS, the cells showed obvious morphological changes and their proliferative capacity was reduced. Under the effect of DEX-HCl, the morphology and proliferation rate of the cells improved significantly. (B) Data analysis. (B1–4) qPCR result of the mRNA expression levels. (B5–8) ELISA result of typical inflammatory factors in the culture medium. (B9, 10) Western blot result. The original image is shown in **Additional Figure 2.** Data are expressed as mean ± SD. Experiments were conducted in quadruplicate. *$P < 0.05$, **$P < 0.01$, ***$P < 0.001$, ****$P < 0.0001$ (one-way analysis of variance followed by Newman-Keuls test). +free: free DOX-HCl in the hydrogel; +lipo: liposome DOX-HCl in the hydrogel. H2-D1: histocompatibility 2, D region locus 1; H2-T23: histocompatibility 2, T region locus 23; HMGB1: high mobility group box 1; IFN-γ: interferon-γ; IL: interleukin; LPS: lipopolysaccharide; ns: not significant; S100a10: S100 calcium-binding protein A10; Tgm1: transglutaminase 1; TNF-α: tumour necrosis factor-α.

Discussion

The optimal injection time for this hydrogel is currently planned to be 10–15 minutes after the formation of the hydrogel precursor, taking three factors into consideration: (1) Gelation speed and time: Although the CS temperature-sensitive hydrogel has slowed down the gelation speed, the delay may cause needle blockage due to incomplete cross-linking, and therefore the injection time should not be too late. (2) Purpose of application: One of the properties envisaged for this hydrogel is the ability to be applied to special shaped wounds such as narrow voids, with the aim of allowing the material to self-adjust to its optimal form in response to the environment in which it is placed, and therefore it should not be injected too late, but earlier than the time of complete gelation. (3) Clinical adaptability: Considering the comfort of the patient and the difficulty of the surgeon to perform the operation, the injection time of the hydrogel precursor should be completed before the gelling time.

The pore structure of liposome-loaded hydrogels becoming more pronounced may be a complex alteration involving the interaction of multiple factors. Specifically, these include the following: (1) release or dissolution of liposomes: liposomes loaded in a hydrogel may release their drug-carrying components or dissolve within the hydrogel, potentially forming new pores to enlarge existing ones, thus increasing the number and size of pores. (2) Structural changes of the hydrogel: loading liposomes may lead to changes in the structure of the hydrogel. Liposomes occupy some positions in the hydrogel matrix, which may lead to fracture or relaxation of part of the hydrogel network, resulting in the formation of more dense pores. (3) Interaction of loading system: Physical or chemical interactions may occur between the hydrogel and the loaded liposomes, such as intermolecular forces, electrostatic interactions, or hydrogen bonding, etc. These interactions may lead to changes in the structure of the hydrogel network, which may affect the distribution and size of the pores. (4) Drug release kinetics: drug release from the loaded liposomes may also lead to changes in the local structure within the hydrogel, including the formation and expansion of pores, especially during the initial rapid release phase of drug release. In conclusion, liposome drug loading into the hydrogel has a benign effect on hydrogel pores .

The mechanism of drug release from drug-loaded liposomal hydrogels usually involves multiple processes, which depend mainly on the nature of the liposomes and the hydrogels themselves, as well as on the interactions between them. (1) Hydrogels typically have a polymeric three-dimensional network structure that creates complex pores, and these pore structures temporarily store the drug and directly affect the rate of drug release. (2) Liposomes themselves have the ability to control drug release, and after being dispersed and immobilised into the network of the hydrogel, they are also equivalent to dispersing the drug uniformly in the hydrogel. (3) Usually, the drug diffuses from the liposome into the hydrogel through the liposome-hydrogel interface, and then diffuses outward into the release medium through the pores of the hydrogel. If the material itself can be degraded, drug release may be affected by multiple aspects of drug dissolution and carrier dissolution. (4) Environmental factors may also affect drug release, for example, the pH, ionic strength and temperature of the release medium can affect the stability of the hydrogel and the rate of drug release. In conclusion, drug-loaded liposome hydrogels are suitable for drug delivery systems that require long-term or controlled release, which can improve drug bioavailability, reduce side effects, enhance drug stability and prolong drug half-life.

In the present study, the reason for the better anti-inflammatory effect in the +lipo group than in the +free group was probably related to two aspects: on the one hand, it was the naturally occurring biotargeting and biodistribution properties of liposomal drugs. Liposomes, as an effective drug delivery system, enhanced the targeting and biodistribution of drugs to cells. DEX-HCl, when loaded into liposomes, could be more easily targeted to the inflammation site or target cells, thus enhancing its anti-inflammatory effect. In contrast, free DEX-HCl may be more rapidly metabolised within the extracellular environment or diffused to non-therapeutic targets, leading to a reduction in its anti-inflammatory effect. The other aspect was the controlled release and sustained release properties of liposomal drugs. Liposomes served as carriers of the drug and could control the rate of release and duration of action of the drug. This means that DEX-HCl loaded into liposomes can maintain its effective concentration for a longer period of time, thus continuously suppressing the inflammatory response. Free DEX-HCl, on the other hand, may not be able to maintain its anti-inflammatory effect effectively because of factors such as its short half-life.

However, there were also abnormal data, such as why the +free group had almost no effect on the reduction of TNF-α expression, and it was speculated that the possible reason was that the biodistribution and metabolic properties of free DEX-HCl resulted in insufficient concentration in the target cells at the site of inflammation to effectively inhibit inflammation, and that a higher dose might be required to achieve the effect of TNF-α inhibition. And in the free state, such long-term high doses might lead to more adverse reactions or side effects, limiting the feasibility of its application. Thus, it was demonstrated side by side that loading the drug into liposomes could be effective in improving its efficacy and safety in the treatment of inflammation, especially by enhancing targeting and prolonging the duration of the drug.

When investigating the feasibility of injectable thermoreactive hydrogels for the treatment of encephalitis, similar experimental animal studies can be drawn upon for reference. For example, Researchers investigated the effects of a therapeutic material similar to a body temperature-responsive hydrogel in *in vivo* models of encephalitis.[58-61] They found that the material was able to significantly reduce the inflammatory response and promote neuroregeneration in infected brain regions. These findings support the potential for the application of temperature-sensitive therapeutic strategies in the treatment of neuroinflammatory diseases. Although their study may differ from the specific materials and therapeutic mechanisms

applied in this study, these results provide theoretical support for our study, suggesting that injectable temperature-responsive hydrogels may have similar positive effects in encephalitis treatment.

On the other hand, natural polymeric temperature-sensitive biomaterials[62-65] similar to the present study were used to treat *in vivo* models of brain abnormalities. The results showed that these materials were able to form gels at high temperatures, which significantly reduced the degree of brain nerve inflammation, promoted the restoration of local neurological functions, and aided in the recovery of neurological diseases. These studies further support the potential of temperature-sensitive therapeutic strategies for neuroprotection and treatment, providing an experimental basis and scientific rationale for our research. By combining the results of these experimental studies, we can speculate that injectable thermoreactive hydrogels may demonstrate potential therapeutic advantages in encephalitis treatment through similar mechanisms and effects. Future studies will further explore the feasibility and safety of this technology in clinical applications.

Herein, we prepared DEX-HCl encapsulated from cationic liposomes, which can be loaded into CS temperature-sensitive hydrogels for the ongoing treatment of encephalitis. It is envisaged that a dural injection of a hydrogel precursor material through a cranial defect would allow for the formation of a stable hydrogel *in situ* in the brain environment. DEX-HCl itself can inhibit encephalitis symptoms, and after being encapsulated by liposomes, it can realize the sustained-release delivery of nanomedicines, so as to achieve long-term anti-inflammatory goals. Overall, this strategy focuses on regulating the subtype transformation of astrocytes in the CNS and treating neuroinflammation on the one hand, and on the other hand, it cleverly combines sustained-release nanodrugs with breakthroughs in skull obstruction, which provides a reliable *in vitro* basis for the treatment of anti-inflammatory drugs in the future. However, the design is not perfect, and there are still problems to be solved, such as how the broken cranial trauma should be protected, and how the more delicate brain injection should be operated, etc., which need to be meticulously explored afterwards.

Author contributions

JL, YW, HZ, and YY in conceived and designed this study. YG and YYin generated, collected and summarised the data. YYin, HZ, and JL analysed and interpreted the data. YYang, JC, BC, and PL checked and touched up the manuscript. The manuscript was written with contributions from all the authors. All the authors have given approval to the final version of the manuscript.

Financial support

This study was financially supported by the National Natural Science Foundation of China (Nos. 52302343, 81825007), Beijing Outstanding Young Scientist Program (No. BJJWZYJH01201910025030), Youth Beijing Scholar Program (No. 010), Beijing Institute of Technology Teli Young Fellow Program (No. RCPT-20220029), and the Beijing Institute of Technology Research Fund Program for Young Scholars (Nos. XSQD-6120220130, XSQD-202213001).

Acknowledgement

None.

Conflicts of interest statement

The authors declare no competing financial interest.

Additional files

Additional Figure 1: The mRNA expression levels of inflammation-related genes were investigated under different LPS concentrations.

Additional Figure 2: The original image of HMGB1 protein expression level.

1. Bellotti, E.; Schilling, A. L.; Little, S. R.; Decuzzi, P. Injectable thermoresponsive hydrogels as drug delivery system for the treatment of central nervous system disorders: A review. *J Control Release.* **2021,** *329*, 16-35.
2. Obermeier, B.; Daneman, R.; Ransohoff, R. M. Development, maintenance and disruption of the blood-brain barrier. *Nat Med.* **2013,** *19*, 1584-1596.
3. Venkatesan, A.; Michael, B. D.; Probasco, J. C.; Geocadin, R. G.; Solomon, T. Acute encephalitis in immunocompetent adults. *Lancet.* **2019,** *393*, 702-716.
4. GBD 2015 Neurological Disorders Collaborator Group. Global, regional, and national burden of neurological disorders during 1990-2015: a systematic analysis for the Global Burden of Disease Study 2015. *Lancet Neurol.* **2017,** *16*, 877-897.
5. Cheng, Y.; Tran Minh, N.; Tran Minh, Q.; Khandelwal, S.; Clapham, H. E. Estimates of Japanese Encephalitis mortality and morbidity: A systematic review and modeling analysis. *PLoS Negl Trop Dis.* **2022,** *16*, e0010361.
6. World Health Organization. Why encephalitis matters? Report of the virtual meeting, 28-29 June 2022. https://www.who.int/publications/i/item/9789240069176. Accessed July 13, 2024.
7. GBD 2016 Neurology Collaborators. Global, regional, and national burden of neurological disorders, 1990-2016: a systematic analysis for the Global Burden of Disease Study 2016. *Lancet Neurol.* **2019,** *18*, 459-480.
8. Nosadini, M.; Thomas, T.; Eyre, M.; Anlar, B.; Armangue, T.; Benseler, S. M.; Cellucci, T.; Deiva, K.; Gallentine, W.; Gombolay, G.; Gorman, M. P.; Hacohen, Y.; Jiang, Y.; Lim, B. C.; Muscal, E.; Ndondo, A.; Neuteboom, R.; Rostásy, K.; Sakuma, H.; Sharma, S.; Tenembaum, S. N.; Van Mater, H. A.; Wells, E.; Wickstrom, R.; Yeshokumar, A. K.; Irani, S. R.; Dalmau, J.; Lim, M.; Dale, R. C. International consensus recommendations for the treatment of pediatric NMDAR antibody encephalitis. *Neurol Neuroimmunol Neuroinflamm.* **2021,** *8*, e1052.
9. Smeyne, R. J.; Noyce, A. J.; Byrne, M.; Savica, R.; Marras, C. Infection and risk of Parkinson's disease. *J Parkinsons Dis.* **2021,** *11*, 31-43.
10. Ray, S. T. J.; Abdel-Mannan, O.; Sa, M.; Fuller, C.; Wood, G. K.; Pysden, K.; Yoong, M.; McCullagh, H.; Scott, D.; McMahon, M.; Thomas, N.; Taylor, M.; Illingworth, M.; McCrea, N.; Davies, V.; Whitehouse, W.; Zuberi, S.; Guthrie, K.; Wassmer, E.; Shah, N.; Baker, M. R.; Tiwary, S.; Tan, H. J.; Varma, U.; Ram, D.; Avula, S.; Enright, N.; Hassell, J.; Ross Russell, A. L.; Kumar, R.; Mulholland, R. E.; Pett, S.; Galea, I.; Thomas, R. H.; Lim, M.; Hacohen, Y.; Solomon, T.; Griffiths, M. J.; Michael, B. D.; Kneen, R.; CoroNerve study group. Neurological manifestations of SARS-CoV-2 infection in hospitalised children and adolescents in the UK: a prospective national cohort study. *Lancet Child Adolesc Health.* **2021,** *5*, 631-641.

11. Pilotto, A.; Masciocchi, S.; Volonghi, I.; Crabbio, M.; Magni, E.; De Giuli, V.; Caprioli, F.; Rifino, N.; Sessa, M.; Gennuso, M.; Cotelli, M. S.; Turla, M.; Balducci, U.; Mariotto, S.; Ferrari, S.; Ciccone, A.; Fiacco, F.; Imarisio, A.; Risi, B.; Benussi, A.; Premi, E.; Focà, E.; Caccuri, F.; Leonardi, M.; Gasparotti, R.; Castelli, F.; Zanusso, G.; Pezzini, A.; Padovani, A. Clinical presentation and outcomes of severe acute respiratory syndrome coronavirus 2-related encephalitis: the ENCOVID multicenter study. *J Infect Dis.* **2021,** *223,* 28-37.
12. Matthews, E.; Beckham, J. D.; Piquet, A. L.; Tyler, K. L.; Chauhan, L.; Pastula, D. M. Herpesvirus-associated encephalitis: an update. *Curr Trop Med Rep.* **2022,** *9,* 92-100.
13. Stahl, J. P.; Mailles, A. Herpes simplex virus encephalitis update. *Curr Opin Infect Dis.* **2019,** *32,* 239-243.
14. Gurgel Assis, M. S.; Fernandes Pedrosa, T. C.; de Moraes, F. S.; Caldeira, T. G.; Pereira, G. R.; de Souza, J.; Ruela, A. L. M. Novel insights to enhance therapeutics with acyclovir in the management of herpes simplex encephalitis. *J Pharm Sci.* **2021,** *110,* 1557-1571.
15. Nance, E.; Pun, S. H.; Saigal, R.; Sellers, D. L. Drug delivery to the central nervous system. *Nat Rev Mater.* **2022,** *7,* 314-331.
16. Wang, T.; Lei, H.; Li, X.; Yang, N.; Ma, C.; Li, G.; Gao, X.; Ge, J.; Liu, Z.; Cheng, L.; Chen, G. Magnetic targeting nanocarriers combined with focusing ultrasound for enhanced intracerebral hemorrhage therapy. *Small.* **2023,** *19,* e2206982.
17. Yokel, R. A. Nanoparticle brain delivery: a guide to verification methods. *Nanomedicine (Lond).* **2020,** *15,* 409-432.
18. Liu, J.; Sun, M.; Li, Z.; Xiang, H.; Wang, Q.; Xin, X.; Shen, Y. Catalytic nanoreactors promote GLUT1-mediated BBB permeation by generating nitric oxide for potentiating glioblastoma ferroptosis. *Chem Eng J.* **2024,** *483,* 149233.
19. Chen, Y. X.; Wei, C. X.; Lyu, Y. Q.; Chen, H. Z.; Jiang, G.; Gao, X. L. Biomimetic drug-delivery systems for the management of brain diseases. *Biomater Sci.* **2020,** *8,* 1073-1088.
20. Zhang, T. T.; Li, W.; Meng, G.; Wang, P.; Liao, W. Strategies for transporting nanoparticles across the blood-brain barrier. *Biomater Sci.* **2016,** *4,* 219-229.
21. Ren, X.; Xu, R.; Xu, C.; Su, J. Harnessing exosomes for targeted therapy: strategy and application. *Biomater Transl.* **2024,** *5,* 46-58.
22. Guo, H.; Guo, M.; Xia, X.; Shao, Z. Membrane-coated nanoparticles as a biomimetic targeted delivery system for tumour therapy. *Biomater Transl.* **2024,** *5,* 33-45.
23. Li, J.; Zhou, H.; Liu, C.; Zhang, S.; Du, R.; Deng, Y.; Zou, X. Biomembrane-inspired design of medical micro/nanorobots: From cytomembrane stealth cloaks to cellularized Trojan horses. *Aggregate.* **2023,** *4,* e359.
24. Lou, M.; Zhao, Y. Satisfactory therapy results of combining nimustine with nicardipine against glioma at advanced stage. *J Cancer Res Ther.* **2015,** *11,* 1030.
25. Mitchell, M. J.; Billingsley, M. M.; Haley, R. M.; Wechsler, M. E.; Peppas, N. A.; Langer, R. Engineering precision nanoparticles for drug delivery. *Nat Rev Drug Discov.* **2021,** *20,* 101-124.
26. Li, G.; Liu, S.; Chen, Y.; Zhao, J.; Xu, H.; Weng, J.; Yu, F.; Xiong, A.; Udduttula, A.; Wang, D.; Liu, P.; Chen, Y.; Zeng, H. An injectable liposome-anchored teriparatide incorporated gallic acid-grafted gelatin hydrogel for osteoarthritis treatment. *Nat Commun.* **2023,** *14,* 3159.
27. Joshi, N.; Yan, J.; Levy, S.; Bhagchandani, S.; Slaughter, K. V.; Sherman, N. E.; Amirault, J.; Wang, Y.; Riegel, L.; He, X.; Rui, T. S.; Valic, M.; Vemula, P. K.; Miranda, O. R.; Levy, O.; Gravallese, E. M.; Aliprantis, A. O.; Ermann, J.; Karp, J. M. Towards an arthritis flare-responsive drug delivery system. *Nat Commun.* **2018,** *9,* 1275.
28. Wang, C.; Yang, Y.; Cao, Y.; Liu, K.; Shi, H.; Guo, X.; Liu, W.; Hao, R.; Song, H.; Zhao, R. Nanocarriers for the delivery of antibiotics into cells against intracellular bacterial infection. *Biomater Sci.* **2023,** *11,* 432-444.
29. Su, Y.; Fan, X.; Pang, Y. Nano-based ocular drug delivery systems: an insight into the preclinical/clinical studies and their potential in the treatment of posterior ocular diseases. *Biomater Sci.* **2023,** *11,* 4490-4507.
30. Wang, Q.; Jiang, N.; Fu, B.; Huang, F.; Liu, J. Self-assembling peptide-based nanodrug delivery systems. *Biomater Sci.* **2019,** *7,* 4888-4911.
31. Pape, K.; Tamouza, R.; Leboyer, M.; Zipp, F. Immunoneuropsychiatry - novel perspectives on brain disorders. *Nat Rev Neurol.* **2019,** *15,* 317-328.
32. Waltl, I.; Kalinke, U. Beneficial and detrimental functions of microglia during viral encephalitis. *Trends Neurosci.* **2022,** *45,* 158-170.
33. Ma, X.; Gao, F.; Su, W.; Ran, Y.; Bilalijiang, T.; Tuolhen, Y.; Tian, G.; Ye, L.; Feng, Z.; Xi, J.; Liu, Z. Multifunctional injectable hydrogel promotes functional recovery after stroke by modulating microglial polarization, angiogenesis and neuroplasticity. *Chem Eng J.* **2023,** *464,* 142520.
34. Zheng, W.; Zhao, K.; Song, L.; Qian, Z.; Liu, W.; Zhu, Y.; Mao, Z.; Gao, C. ROS-scavenging microgels containing PTPσ receptor modulatory peptides synergistically alleviate inflammation and promote functional recovery post stroke. *Chem Eng J.* **2024,** *483,* 149225.
35. Colombo, E.; Farina, C. Astrocytes: Key Regulators of Neuroinflammation. *Trends Immunol.* **2016,** *37,* 608-620.
36. Liu, Y.; Zhang, F.; Long, L.; Li, J.; Liu, Z.; Hu, C.; Chen, X.; Zan, X.; Xu, J.; Wang, Y. Dual-function hydrogels with sequential release of GSK3β inhibitor and VEGF inhibit inflammation and promote angiogenesis after stroke. *Chem Eng J.* **2022,** *433,* 133671.
37. Mei, B.; Li, J.; Zuo, Z. Dexmedetomidine attenuates sepsis-associated inflammation and encephalopathy via central α2A adrenoceptor. *Brain Behav Immun.* **2021,** *91,* 296-314.
38. Venkatesan, A.; Tunkel, A. R.; Bloch, K. C.; Lauring, A. S.; Sejvar, J.; Bitnun, A.; Stahl, J. P.; Mailles, A.; Drebot, M.; Rupprecht, C. E.; Yoder, J.; Cope, J. R.; Wilson, M. R.; Whitley, R. J.; Sullivan, J.; Granerod, J.; Jones, C.; Eastwood, K.; Ward, K. N.; Durrheim, D. N.; Solbrig, M. V.; Guo-Dong, L.; Glaser, C. A.; International Encephalitis Consortium. Case definitions, diagnostic algorithms, and priorities in encephalitis: consensus statement of the international encephalitis consortium. *Clin Infect Dis.* **2013,** *57,* 1114-1128.
39. Najjar, S.; Pearlman, D. M.; Alper, K.; Najjar, A.; Devinsky, O. Neuroinflammation and psychiatric illness. *J Neuroinflammation.* **2013,** *10,* 43.
40. Wang, K.; Chen, Y.; Ahn, S.; Zheng, M.; Landoni, E.; Dotti, G.; Savoldo, B.; Han, Z. GD2-specific CAR T cells encapsulated in an injectable hydrogel control retinoblastoma and preserve vision. *Nat Cancer.* **2020,** *1,* 990-997.
41. Tischner, D.; Reichardt, H. M. Glucocorticoids in the control of neuroinflammation. *Mol Cell Endocrinol.* **2007,** *275,* 62-70.
42. Zamanian, J. L.; Xu, L.; Foo, L. C.; Nouri, N.; Zhou, L.; Giffard, R. G.; Barres, B. A. Genomic analysis of reactive astrogliosis. *J Neurosci.* **2012,** *32,* 6391-6410.
43. Liddelow, S. A.; Guttenplan, K. A.; Clarke, L. E.; Bennett, F. C.; Bohlen, C. J.; Schirmer, L.; Bennett, M. L.; Münch, A. E.; Chung, W. S.; Peterson, T. C.; Wilton, D. K.; Frouin, A.; Napier, B. A.; Panicker, N.; Kumar, M.; Buckwalter, M. S.; Rowitch, D. H.; Dawson, V. L.; Dawson, T. M.; Stevens, B.; Barres, B. A. Neurotoxic reactive astrocytes are

induced by activated microglia. *Nature.* **2017,** *541,* 481-487.
44. Sun, Y. B.; Zhao, H.; Mu, D. L.; Zhang, W.; Cui, J.; Wu, L.; Alam, A.; Wang, D. X.; Ma, D. Dexmedetomidine inhibits astrocyte pyroptosis and subsequently protects the brain in in vitro and in vivo models of sepsis. *Cell Death Dis.* **2019,** *10,* 167.
45. Tseng, T. C.; Tao, L.; Hsieh, F. Y.; Wei, Y.; Chiu, I. M.; Hsu, S. H. An Injectable, self-healing hydrogel to repair the central nervous system. *Adv Mater.* **2015,** *27,* 3518-3524.
46. Li, Q.; Shao, X.; Dai, X.; Guo, Q.; Yuan, B.; Liu, Y.; Jiang, W. Recent trends in the development of hydrogel therapeutics for the treatment of central nervous system disorders. *NPG Asia Mater.* **2022,** *14,* 14.
47. Zhan, W.; Wang, C. H. Convection enhanced delivery of liposome encapsulated doxorubicin for brain tumour therapy. *J Control Release.* **2018,** *285,* 212-229.
48. Chen, C.; Sun-Waterhouse, D.; Zhao, J.; Zhang, Y.; Waterhouse, G. I. N.; Lin, L.; Zhao, M.; Sun, W. Method for loading liposomes with soybean protein isolate hydrolysate influences the antioxidant efficiency of liposomal systems: Adding after liposomes formation or before lipid film hydration. *Food Hydrocoll.* **2022,** *129,* 107629.
49. Abrami, M.; Siviello, C.; Grassi, G.; Larobina, D.; Grassi, M. Investigation on the thermal gelation of Chitosan/β-Glycerophosphate solutions. *Carbohydr Polym.* **2019,** *214,* 110-116.
50. Tang, S.; Yang, J.; Lin, L.; Peng, K.; Chen, Y.; Jin, S.; Yao, W. Construction of physically crosslinked chitosan/sodium alginate/calcium ion double-network hydrogel and its application to heavy metal ions removal. *Chem Eng J.* **2020,** *393,* 124728.
51. Huang, W.; Cheng, S.; Wang, X.; Zhang, Y.; Chen, L.; Zhang, L. Noncompressible hemostasis and bone regeneration induced by an absorbable bioadhesive self-healing hydrogel. *Adv Funct Mater.* **2021,** *31,* 2009189.
52. Kim, H. J.; Choi, B. H.; Jun, S. H.; Cha, H. J. Sandcastle worm-inspired blood-resistant bone graft binder using a sticky mussel protein for augmented in vivo bone regeneration. *Adv Healthc Mater.* **2016,** *5,* 3191-3202.
53. Magdanz, V.; Khalil, I. S. M.; Simmchen, J.; Furtado, G. P.; Mohanty, S.; Gebauer, J.; Xu, H.; Klingner, A.; Aziz, A.; Medina-Sánchez, M.; Schmidt, O. G.; Misra, S. IRONSperm: sperm-templated soft magnetic microrobots. *Sci Adv.* **2020,** *6,* eaba5855.
54. Ren, S.; Dai, Y.; Li, C.; Qiu, Z.; Wang, X.; Tian, F.; Zhou, S.; Liu, Q.; Xing, H.; Lu, Y.; Chen, X.; Li, N. Pharmacokinetics and pharmacodynamics evaluation of a thermosensitive chitosan based hydrogel containing liposomal doxorubicin. *Eur J Pharm Sci.* **2016,** *92,* 137-145.
55. Cohen, J. The immunopathogenesis of sepsis. *Nature.* **2002,** *420,* 885-891.
56. Soares, D. G.; Zhang, Z.; Mohamed, F.; Eyster, T. W.; de Souza Costa, C. A.; Ma, P. X. Simvastatin and nanofibrous poly(l-lactic acid) scaffolds to promote the odontogenic potential of dental pulp cells in an inflammatory environment. *Acta Biomater.* **2018,** *68,* 190-203.
57. Zhang, H. Y.; Wang, Y.; He, Y.; Wang, T.; Huang, X. H.; Zhao, C. M.; Zhang, L.; Li, S. W.; Wang, C.; Qu, Y. N.; Jiang, X. X. A1 astrocytes contribute to murine depression-like behavior and cognitive dysfunction, which can be alleviated by IL-10 or fluorocitrate treatment. *J Neuroinflammation.* **2020,** *17,* 200.
58. Albashari, A.; He, Y.; Zhang, Y.; Ali, J.; Lin, F.; Zheng, Z.; Zhang, K.; Cao, Y.; Xu, C.; Luo, L.; Wang, J.; Ye, Q. Thermosensitive bFGF-modified hydrogel with dental pulp stem cells on neuroinflammation of spinal cord injury. *ACS Omega.* **2020,** *5,* 16064-16075.
59. Li, Y.; Wang, M.; Sun, M.; Wang, X.; Pei, D.; Lei, B.; Li, A. Engineering antioxidant poly (citrate-gallic acid)-Exosome hybrid hydrogel with microglia immunoregulation for Traumatic Brain Injury-post neuro-restoration. *Compos B Eng.* **2022,** *242,* 110034.
60. Zhang, M.; Zhang, R.; Chen, H.; Zhang, X.; Zhang, Y.; Liu, H.; Li, C.; Chen, Y.; Zeng, Q.; Huang, G. Injectable supramolecular hybrid hydrogel delivers IL-1β-stimulated exosomes to target neuroinflammation. *ACS Appl Mater Interfaces.* **2023,** *15,* 6486-6498.
61. Liu, Y.; Tan, Y.; Cheng, G.; Ni, Y.; Xie, A.; Zhu, X.; Yin, C.; Zhang, Y.; Chen, T. Customized intranasal hydrogel delivering methylene blue ameliorates cognitive dysfunction against Alzheimer's disease. *Adv Mater.* **2024,** *36,* e2307081.
62. Yao, M.; Chen, Y.; Zhang, J.; Gao, F.; Ma, S.; Guan, F. Chitosan-based thermosensitive composite hydrogel enhances the therapeutic efficacy of human umbilical cord MSC in TBI rat model. *Mater Today Chem.* **2019,** *14,* 100192.
63. Xu, D.; Qiao, T.; Wang, Y.; Wang, Q. S.; Cui, Y. L. Alginate nanogels-based thermosensitive hydrogel to improve antidepressant-like effects of albiflorin via intranasal delivery. *Drug Deliv.* **2021,** *28,* 2137-2149.
64. Mahajan, S.; Nangare, S.; Chaudhari, A.; Patil, G. Synthesis of chitosan-graphene oxide thermosensitive in situ hydrogel for nasal delivery of rasagiline mesylate: in-vitro-ex vivo characterization. *J Drug Deliv Sci Technol.* **2024,** *95,* 105549.
65. Gholizadeh, H.; Cheng, S.; Pozzoli, M.; Messerotti, E.; Traini, D.; Young, P.; Kourmatzis, A.; Ong, H. X. Smart thermosensitive chitosan hydrogel for nasal delivery of ibuprofen to treat neurological disorders. *Expert Opin Drug Deliv.* **2019,** *16,* 453-466.

Received: May 31, 2024
Revised: July 10, 2024
Accepted: August 30, 2024
Available online: September 28, 2024